

Sodium Chloride Concentration Effects on General CO₂ Corrosion Mechanisms

H. Fang,^{*} B. Brown,^{†,*} and S. Nešić^{*}

ABSTRACT

The general carbon dioxide (CO₂) corrosion rates of C1018 (UNS G10180) carbon steel have been measured for sodium chloride (NaCl) concentrations 3 wt% to 25 wt% at 20°C, pH 4.0, 5.0, and 6.0. Experimental results showed that high salt concentrations decreased the general CO₂ corrosion rate significantly and nonlinearly. Potentiodynamic sweep analysis shows that both cathodic and anodic processes were retarded. Flow velocity effects on general CO₂ corrosion rate were minimized as a result of an increase of salt concentration. No effect of high salt concentration on initiation of localized attack was detected.

KEY WORDS: carbon steel, chloride, CO₂ corrosion, high salt concentration, linear polarization resistance, localized corrosion, pitting attack, potentiodynamic sweep

INTRODUCTION

Carbon dioxide (CO₂, sweet) corrosion is a complicated process and is affected by many different parameters (for example: temperature, CO₂ partial pressure, pH), which make it difficult for prediction models to provide accurate results. A large body of research has been conducted in this field over the last three decades. The first significant CO₂ corrosion model, introduced by de Waard and Milliams in 1975, iden-

tified the combined effect of CO₂ partial pressure and temperature on the corrosion rate as the key parameters in CO₂ corrosion.¹ Since then many other parameters have been uncovered such as pH, velocity, etc.²⁻⁷ However, CO₂ corrosion in solutions with high salt concentrations has not been addressed adequately.

The most previous research related to the effect of salt on CO₂ corrosion focused on the effect of chloride ion concentration in localized corrosion. For example, Sun, et al., investigated the effect of Cl⁻ on localized corrosion in wet gas pipelines.⁸ Ma, et al., also studied the influence of chloride ions on the corrosion of iron.⁹ Both investigations concluded that chlorides accelerate localized corrosion. However, the effect of salt content on general CO₂ corrosion was not even mentioned in either paper.

The reality in the field is that dissolved salts (sometimes at very high concentration) are present in water recovered from oil and gas wells. For example, a water analysis from a Texas gas well is shown in Table 1. Salt content is about 23 wt%, which is typical for this location. It is not uncommon that salt crystals are seen in the production tubing in Texas, meaning salt concentration could be near saturation. Therefore, it is important to know if this high content of salt has effects on CO₂ corrosion of carbon steel or not.

A series of experiments looking into high salt concentration effects on CO₂ corrosion has been performed and reported for low temperature, 5°C.¹⁰ A significant salt retardation effect on general CO₂ corrosion rate was observed during those experiments. Adsorption of chlorides was suspected to be the reason for this behavior. The present study focused on

Submitted for publication: April 7, 2010. Revised and accepted: August 17, 2010. Preprint available online: February 5, 2013, <http://dx.doi.org/10.5006/0222>. Part 1 of this manuscript appeared in *Corrosion* 67, 1 (2011), p. 015001-1-015001-12, doi: <http://dx.doi.org/10.5006/1.3546847>.

[†] Corresponding author.

^{*} Institute for Corrosion and Multiphase Technology, 342 West State St., Ohio University, Athens, Ohio 45701.

TABLE 1
Water Analysis Summary for a Texan Gas Well

Compound	Compound (mg/L)	Concentration (wt%)
NaCl	131,080	13.1
CaCl ₂ ·2H ₂ O	111,510	8.36
MgCl ₂ ·6H ₂ O	50,810	2.39
Total	293,400	23.85

TABLE 2
Chemical Composition of C1018 Carbon Steel (wt%)

C	Si	P	S	Mn	Al	Fe
0.21	0.38	0.09	0.05	0.05	0.01	Balance

clarifying the salt retardation mechanism by conducting more experiments at room temperature, 20°C.

EXPERIMENTAL PROCEDURES

Specimen Preparation

The same type of carbon steel (C1018 [UNS G10180]⁽¹⁾) was used for weight-loss, linear polarization resistance (LPR), electrical impedance spectroscopy (EIS), and potentiodynamic sweep analyses. Rotating cylinder electrodes (RCE) with a surface area of 5.4 cm² (1.27 cm diameter by 1.35 cm length) were used for each test. The chemical composition of the carbon steel is shown in Table 2.

The specimen was polished with silicon carbide (SiC) sand paper before it was tested, and the sand paper grit number used was in the following order: 240, 400, and 600. After polishing, the specimen was immersed in isopropyl alcohol (C₃H₈O) in an ultrasonic cleaner for 1 min to 2 min and then air dried.

Experimental Setup

The experiments were performed in a glass cell, which is shown in Figure 1. A silver/silver chloride (Ag/AgCl, 4 M potassium chloride [KCl]) reference electrode was connected externally to the cell via a Luggin capillary with a porous glass tip. A counter electrode was made of a concentric platinum ring. The test matrix for this experimental series is shown in Table 3.

A glass cell was filled with 2 L of deionized water with the desired concentration of NaCl. Cell temperature was measured by a thermocouple connected to a hot plate. The solution was deoxygenated by purging with CO₂ gas. The solution could be deoxygenated in about 40 min to 1 h of purging. When the desired temperature was attained, the pH of the test solution was adjusted from equilibrium pH (3.8 to 3.9) to the desired pH (4.0, 5.0, 6.0) by adding a deoxygenated sodium bicarbonate (NaHCO₃) solution. Then,

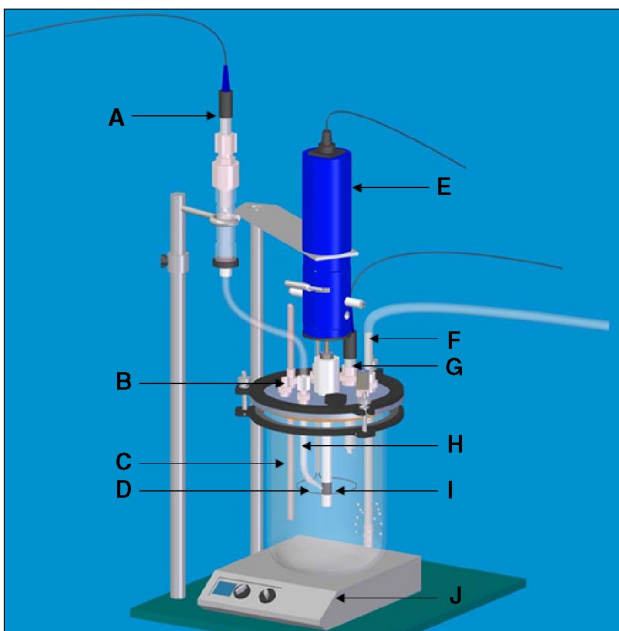


FIGURE 1. Schematic of a glass cell for CO₂ corrosion. (A) Reference electrode, (B) gas outlet, (C) temperature probe, (D) platinum counter electrode, (E) rotator, (F) gas inlet, (G) pH electrode, (H) Luggin capillary, (I) working electrode, and (J) hot plate.

TABLE 3
Test Matrix for CO₂ Experiments

Parameters	Conditions
Total pressure	1 bar
Temperature	20°C
Rotation speed	1,000, 4,000 rpm
NaCl solution	3, 10, 20, 25 wt%
pH	4.0
Material	UNS G10180

the RCE working electrode was put into the solution and all electrical connections were made for corrosion rate monitoring. The rotational speed was set and the open-circuit potential was monitored for 20 min to 60 min for a stable signal before all the electrochemical measurements presented below were carried out.

Measurement Techniques

There are two main groups of techniques that were used to monitor the corrosion process. They are electrochemical measurement and weight-loss measurement.

The electrochemical measurements typically were conducted in the same order. First, LPR was performed to measure the corrosion rate, then the solution resistance was measured by conducting EIS, and last, a potentiodynamic sweep was performed. All electrochemical measurements were made using an electrochemical potentiostat monitoring system.

The LPR technique was used to measure the corrosion rate. The steel sample was polarized at ±5 mV or ±10 mV around the open-circuit potential during

⁽¹⁾ UNS numbers are listed in *Metals and Alloys in the Unified Numbering System*, published by the Society of Automotive Engineers (SAE International) and cosponsored by ASTM International.

the LPR measurement (depending on the level of the inherent electrochemical noise). The scan rate was 0.125 mV/s. What LPR actually measures is polarization resistance, not corrosion rate. Polarization resistance can be converted to corrosion rate from the basic electrochemical theory. The corrosion current density, i_{corr} , (A/m^2) is:

$$i_{corr} = B \times \frac{1}{R_p} \times \frac{1}{A} \quad (1)$$

where R_p is the polarization resistance as measured by LPR. The solution resistance (R_s) measured by EIS needs to be subtracted from the total corrosion resistance. A is the surface area, which is 5.4 cm^2 , and B is the "B value," which can be calculated from Equation (2):

$$B = \frac{\beta_a \beta_c}{2.303(\beta_a + \beta_c)} \quad (2)$$

where β_a and β_c are the anodic and cathodic Tafel slopes, respectively, which can be expressed as:

$$\beta_a = \frac{2.303RT}{\alpha_a F} \quad (3)$$

$$\beta_c = \frac{2.303RT}{\alpha_c F} \quad (4)$$

where T is the absolute temperature in K, R is the universal gas constant (8.314 J/mol K), α_a and α_c are the symmetry factors for anodic and cathodic reactions, respectively. The values of α_a and α_c are typically 1.5 and 0.5, respectively.¹¹ F is Faraday's constant ($96,500\text{ C/eq.}$).

Corrosion rate in mm/y then is calculated by:

$$CR = \frac{m}{Atp} \chi = \frac{i_{corr} M_w}{\rho n F} \chi = 1.16 i_{corr} \quad (5)$$

where m is the metal loss in kg, t is the time in seconds, ρ is the density of the material in kg/m^3 , M_w is the molecular weight of iron in kg/mol , n is the number of electrons exchanged in the electrochemical reaction, and χ is the unit conversion factor.

The potentiodynamic sweep technique was used to investigate the corrosion mechanism. The sweeps were conducted with a scan rate of 0.2 mV/s.

Weight-loss measurement was used to verify the corrosion rate magnitude. At the same test conditions as electrochemical measurements, a pre-weighed RCE was put into the test solution. Typically after 24 h, the sample was taken out of the test solution, rinsed with isopropyl alcohol and wiped with a cloth to remove any salt residue and carbide scales, then air dried and weighed.

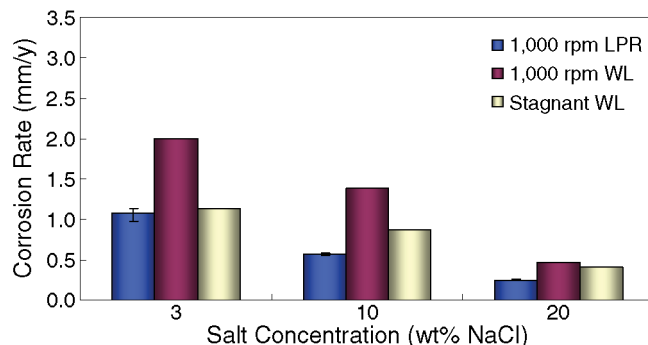


FIGURE 2. LPR and weight-loss corrosion rates in CO_2 purged solutions (pH 4, 20°C, 3 wt%, 10 wt%, 20 wt% NaCl, $B = 12\text{ mV/decade}$).

TABLE 4
B Value Calculations at pH 4, 20°C

NaCl Concentration (wt%)	Weight Loss (mm/y)	R_p (Ω)	Area (cm^2)	B (mV/decade)	$B_{average}$ (mV/decade)
3	2	26.2	5.4	24	
10	1.46	48.9	5.4	33	27
20	0.46	110.8	5.4	24	

RESULTS AND DISCUSSION

Twenty-five glass cell experiments were conducted at 20°C. Some of the tests were repeated several times to check the reproducibility of the results. At the beginning of the experiments, charge-transfer control was assumed to be the main corrosion controlling mechanism under these test conditions. Tafel slopes were calculated based on Equations (3) and (4). The B value derived from the equations was $B = 12\text{ mV}$.

Figure 2 shows the corrosion rate results measured by LPR and weight loss under the following conditions: pH 4, 3 wt% to 20 wt% NaCl, 20°C, stagnant flow, and 1,000 rpm. It is apparent that the corrosion rates measured by these two different methods are not in agreement. The weight-loss results also show some flow effect on the corrosion rates. Therefore, the corrosion mechanism assumed prior to testing this set of conditions was wrong. As it turned out, the corrosion rate was not under pure charge-transfer control, but rather under mixed charge/mass-transfer control. Therefore, it was difficult to derive explicitly the Tafel slopes β_a and β_c from potentiodynamic sweeps for this kind of corrosion mechanism. However, the actual B values can be estimated by comparing the polarization resistance measured by LPR and corrosion rates measured by weight loss. Table 4 shows the calculated B values by using this method. The B values shown there are realistic and correspond to a situation when one of the reactions (in this case cathodic) is limited by mass transfer. Figure 3 shows the LPR and weight-

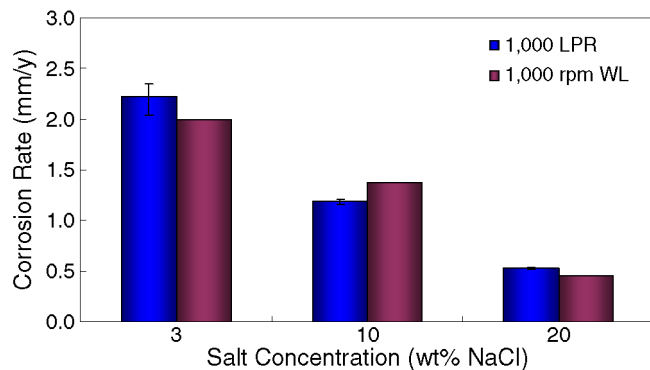


FIGURE 3. LPR (corrected B value) and weight-loss corrosion rates in CO_2 -purged solutions ($\text{pH } 4$, 20°C , 3 wt%, 10 wt%, 20 wt% NaCl , $B = 27 \text{ mV/decade}$).

loss corrosion rates after B value “correction,” i.e., when the average value, $B = 27 \text{ mV/decade}$, is used for all the LPR calculations. As expected, the results agree very well.

Test with 3 wt% NaCl

Figure 4 shows the corrosion rate results measured by LPR at 20°C , pH 4, and 1,000 rpm and 4,000 rpm for a 3 wt% NaCl solution. The LPR corrosion rate is around 2.2 mm/y at 1,000 rpm and 3.3 mm/y at

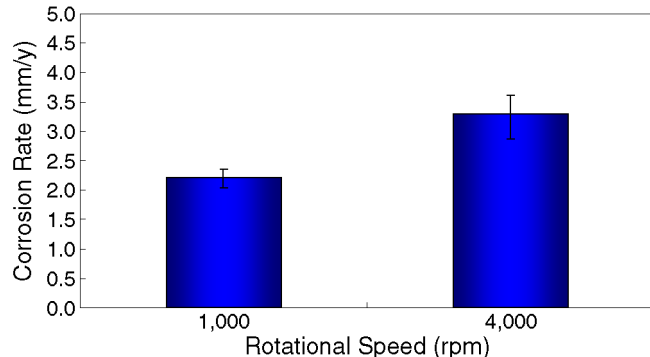


FIGURE 4. Flow velocity effect on LPR corrosion rate in CO_2 -purged solutions ($\text{pH } 4$, 20°C , 1,000 rpm to 4,000 rpm, 3 wt% NaCl).

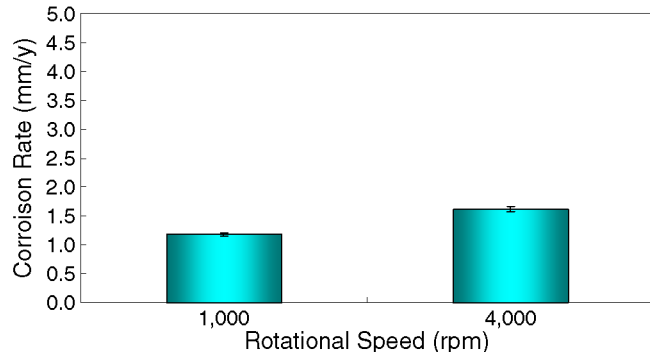


FIGURE 6. Flow velocity effect on LPR corrosion rate in CO_2 -purged solutions ($\text{pH } 4$, 20°C , 1,000 rpm to 4,000 rpm, 10 wt% NaCl).

4,000 rpm. There is a significant difference in the corrosion rates measured at the lower velocity and the higher velocity under these conditions. Figure 5 shows the potentiodynamic sweep results at different flow velocities. The corrosion potential changed with the flow condition because the cathodic corrosion process is under partial mass-transfer control and responded to the increase in velocity.

Test with 10 wt% NaCl

The LPR corrosion rate results are shown in Figure 6 for a 10 wt% NaCl solution. The LPR corrosion rate is around 1.2 mm/y at 1,000 rpm and 1.6 mm/y at 4,000 rpm. Apparently, flow still has an effect on the corrosion rate. A comparison of corrosion rates in 10 wt% NaCl to those in 3 wt% NaCl shows a 50% decrease in the general corrosion rate for all rotational speeds tested, which is similar to the results at 5°C . Figure 7 shows the potentiodynamic sweep results at different rotational speeds. As was observed at 3 wt%, in the case of 10 wt% NaCl , the flow velocity accelerated the corrosion process. But, the flow effect seemed to be mitigated by adding more salt.

Test with 20 wt% NaCl

Figure 8 shows the LPR corrosion rate results for a 20 wt% NaCl solution. The corrosion rate is

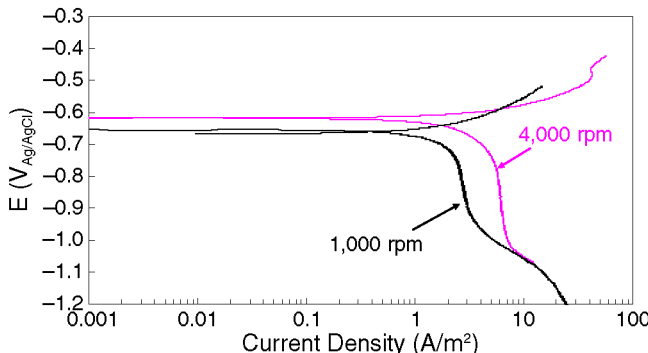


FIGURE 5. Flow velocity effect on potentiodynamic sweep in CO_2 -purged solutions ($\text{pH } 4$, 20°C , 1,000 rpm to 4,000 rpm, 3 wt% NaCl).

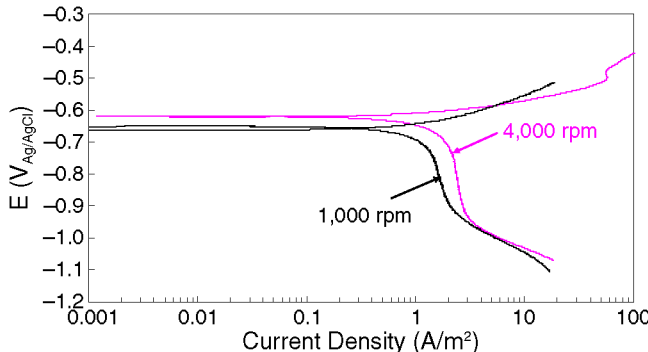


FIGURE 7. Flow velocity effect on potentiodynamic sweep in CO_2 -purged solutions ($\text{pH } 4$, 20°C , 1,000 rpm to 4,000 rpm, 10 wt% NaCl).

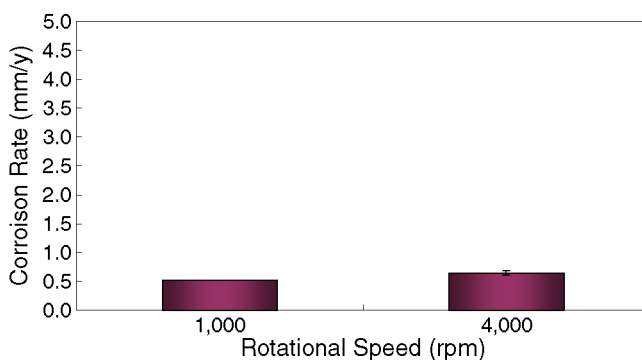


FIGURE 8. Flow velocity effect on LPR corrosion rate in CO_2 -purged solutions (pH 4, 20°C, 1,000 rpm to 4,000 rpm, 20 wt% NaCl).

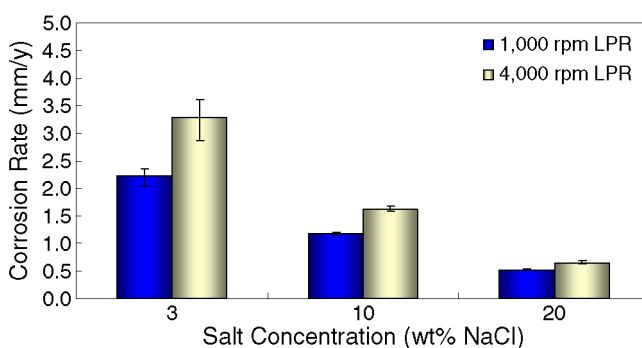


FIGURE 10. Salt effect on LPR corrosion rate in CO_2 -purged solutions (pH 4, 20°C, 1,000, 4,000 rpm, 3 wt%, 10 wt%, and 20 wt% NaCl).

decreased further as compared with the data of 3 wt% and 10 wt% NaCl solutions. Flow velocity effect on LPR corrosion rate continues to become less pronounced. Figure 9 shows the potentiodynamic sweep results. The flow velocity effect on the corrosion process is not significant at this saline concentration, which suggests that the corrosion mechanism gradually changes from mixed charge/mass-transfer control to pure charge-transfer control with the increase of salt concentration.

Summary of Salt Effect on the Corrosion Rate at 20°C

Figure 10 illustrates the NaCl concentration effect on the LPR corrosion rates. It is seen from that figure that NaCl concentration has a significant effect on the corrosion rates. Corrosion rates decrease by 50% as NaCl concentration is increased from 3 wt% to 10 wt%. Corrosion rates can decrease even further by another 50% as the NaCl concentration is increased from 10 wt% to 20 wt%.

The fact that corrosion rates as measured by LPR decrease with increasing salt concentrations can be explained by looking at potentiodynamic sweep results. Figures 11 and 12 show the cathodic and anodic curves at different NaCl concentrations at

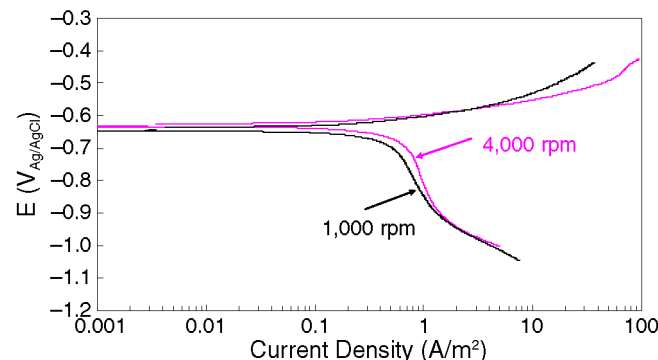


FIGURE 9. Flow velocity effect on potentiodynamic sweep in CO_2 -purged solutions (pH 4, 20°C, 1,000 rpm to 4,000 rpm, 20 wt% NaCl).

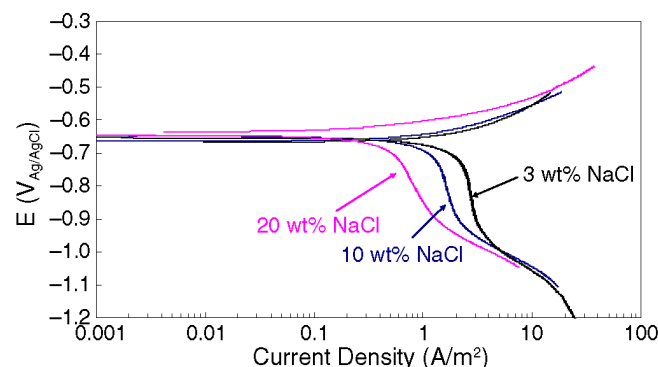


FIGURE 11. Salt effect on potentiodynamic sweep in CO_2 -purged solutions (pH 4, 20°C, 1,000 rpm, 3 wt%, 10 wt%, and 20 wt% NaCl).

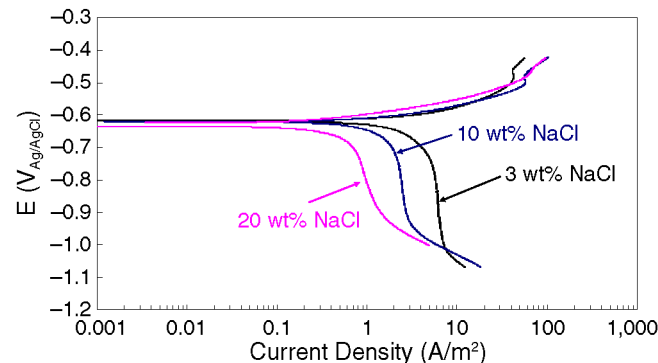


FIGURE 12. Salt effect on potentiodynamic sweep in CO_2 -purged solutions (pH 4, 20°C, 4,000 rpm, 3 wt%, 10 wt%, and 20 wt% NaCl).

1,000 rpm and 4,000 rpm. Independent of the rotational speed, the cathodic curve and the anodic curve show the same trend—both shift to the smaller values as the NaCl concentration is increased. This means that the presence of salt retards both the cathodic and the anodic reactions. This phenomenon is almost identical to what was observed at 5°C.¹⁰ It should be noted that no initiation of localized attack (pitting) was observed in this series of experiments at any salt concentration.

CONCLUSIONS

- ❖ The CO₂ general corrosion rate of carbon steel significantly decreases with the increase of NaCl concentration.
- ❖ With the increase of salt concentration, the general CO₂ corrosion mechanism gradually changes from mixed charge-transfer/limiting current control to pure charge-transfer control.

REFERENCES

1. C. de Waard, D.E. Milliams, *Corrosion* 31, 5 (1975): p. 177.
 2. C. de Waard, D.E. Milliams, "Predictive Model for CO₂ Corrosion Engineering in Wet Natural Gas Pipelines," CORROSION/91, paper no. 577 (Houston, TX: NACE International, 1991).
 3. C. de Waard, U. Lotz, "Prediction of CO₂ Corrosion of Carbon Steel," CORROSION/93, paper no. 69 (Houston, TX: NACE International, 1993).
 4. C. de Waard, U. Lotz, A. Dugstad, "Influence of Liquid Flow Velocity on CO₂ Corrosion: A Semi-Empirical Model," CORROSION/95, paper no. 128 (Houston, TX: NACE, 1995).
 5. L.D.S. Gray, B.G. Anderson, M.J. Danysh, P.R. Tremaine, "Mechanisms of Carbon Steel Corrosion in Brines Containing Dissolved Carbon Dioxide at pH 4," CORROSION/89, paper no. 464 (Houston, TX: NACE, 1989).
 6. L.D.S. Gray, B.G. Anderson, M.J. Danysh, P.R. Tremaine, "Effect of pH and Temperature on the Mechanisms of Carbon Steel Corrosion by Aqueous Carbon Dioxide," CORROSION/90, paper no. 40 (Houston, TX: NACE, 1990).
 7. S. Nešić, J. Postlethwaite, S. Olsen, *Corrosion* 52, 4 (1996): p. 280, doi: <http://dx.doi.org/10.5006/1.3293640>.
 8. Y. Sun, K. George, S. Nešić, "The Effect of Cl⁻ and Acetic Acid on Localized CO₂ Corrosion in Wet Gas Flow," CORROSION/2003, paper no. 03327 (Houston, TX: NACE, 2003).
 9. H.Y. Ma, C. Yang, G.Y. Li, W.J. Guo, S.H. Chen, J.L. Luo, *Corrosion* 59, 12 (2003): p. 1112, doi: <http://dx.doi.org/10.5006/1.3277530>.
 10. H. Fang, S. Nešić, B. Brown, S. Wang, "General CO₂ Corrosion in High Salinity Brines," CORROSION/2006, paper no. 06372 (Houston, TX: NACE, 2006).
 11. J.O'M. Bockris, D. Drazic, A.R. Despic, *Electrochim. Acta* 4 (1961): p. 325.
-